

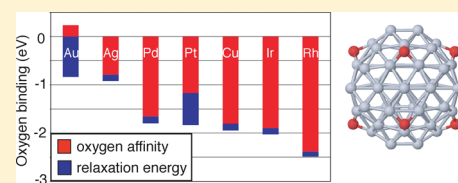
Role of Geometric Relaxation in Oxygen Binding to Metal Nanoparticles

Chun-Yaung Lu and Graeme Henkelman*

Department of Chemistry and Biochemistry, The University of Texas at Austin, Austin, Texas 78712-0165, United States

ABSTRACT: Better oxygen reduction catalysts are needed to improve the efficiency and lower the cost of fuel cells. Metal nanoparticles are good candidates because their catalytic properties can differ from bulk metals. Using density functional theory calculations, we studied the geometric relaxation of metal nanoparticles upon oxygen binding. Because bound oxygen species are intermediates in the oxygen reduction reaction, the binding of oxygen can be correlated to catalytic activity. Our results show that Pt and Au are unique in that they exhibit a larger structural deformation than other metals, which is pronounced for particles with fewer than 100 atoms. The structural deformation induced by atomic oxygen binding stabilizes the oxidized state and thus reduces the catalytic activity of Pt-based random alloys. We show that the catalytic activity of Pt can be improved by forming alloys with less deformable metals.

SECTION: Nanoparticles and Nanostructures



Fuel cells are promising power sources, but the performance of current proton-exchange membrane fuel cells is limited by several material issues. Among them is the choice of catalyst at the cathode. The best platinum-based catalysts still show significant overpotential losses. Inefficiencies combined with the high price of platinum makes the widespread use of these fuel cells impractical. Thus, we are motivated to search for better and less-expensive alternatives. Bimetallic alloys, for example, provide a particularly exciting possibility for tuning the reactivity of catalysts. In certain cases, new properties appear in alloy systems that are absent in the constituent metals.^{1,2} In the system that we are studying, Pt-based bimetallic nanoparticles used to catalyze the oxygen reduction reaction (ORR) have been shown³ to exhibit synergetic effects when alloyed with Pd (Figure 1).

Computer modeling has become a powerful tool in screening potential candidates of fuel cell catalysts. Using the binding energy of atomic oxygen as a indicator of ORR activity in metal catalysts was proposed by Bligaard et al.⁴ For metals other than Ag and Au, a weaker oxygen binding energy would increase the ORR activity. While a large portion of recent studies focus on the electronic properties of catalysts, the geometric contribution to the catalytic activity has received less attention. From a chemical point of view, changes in binding site geometry should also play an important role in chemical reactions. This is especially important for metal nanoparticles (NPs) in the nanometer or subnanometer size regime. For Pt-based random alloy NPs with oxygen adsorbed on the metal surface, a structural deformation stabilizes the oxidized states and thus reduces the catalytic activity. Upon the basis of this principle, we discuss the possibility of improving catalytic performance by making alloys with less deformable metals.

The binding energy of atomic oxygen on various metallic surfaces was calculated with density function theory (DFT) using the

generalized gradient approximation (GGA) functional PW91^{5,6} as implemented in the VASP code.^{7–9} Valence electrons were treated explicitly in the Kohn–Sham⁷ equations, and core electrons were described by pseudopotentials with the projector augmented wave (PAW) method.^{10,11} A plane-wave basis set with an energy cutoff of 251 eV was used for all calculations except for particles containing Cu, in which it was raised to 274 eV. Spin polarization was tested in all cases and used as needed. Stable structures were calculated using force-based energy minimization. zGeometries were considered optimized when the force on each atom was less than 0.003 eV/Å.

Single-crystal surfaces were modeled with four-layer slabs containing nine atoms per layer in a $p(3 \times 3)$ unit cell of the (111) surface (see Figure 2). Because the (111) facet has the weakest oxygen binding sites, it is considered the most ORR-active. In our calculations, an oxygen atom was adsorbed on one of the face-centered cubic (FCC) hollows. A surface of this size and a vacuum gap of at least 10 Å between slabs was used to isolate adsorbed oxygen atoms from their periodic images. A $(3 \times 3 \times 1)$ Monkhost–Pack k -point mesh was used to sample the Brillouin zone.¹² In all calculations, the bottom two layers of the slab were held frozen in their lattice positions.

NPs were modeled as FCC crystallites in the shape of a truncated octahedron (Figure 2). The truncated octahedron was found to be the most stable structure for a pure Pt particle of 79 atoms (denoted as NP79). The particles were contained in a cubic box of side length 20 (NP79) or 23 Å (NP140). Because the particles were isolated by a vacuum gap in all directions, a single Γ -point sampling of the Brillouin zone was used. Eight oxygen atoms were adsorbed on the central FCC hollows of

Received: March 19, 2011

Accepted: May 4, 2011

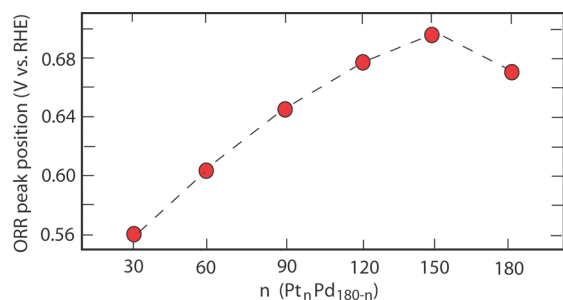


Figure 1. Experimental ORR peak current position for various $\text{Pt}_n\text{Pd}_{180-n}$ compositions. Figure reproduced from Ye and Crooks.³

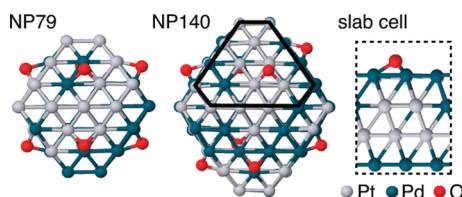


Figure 2. Structures of Pd/Pt random alloy nanoparticles (NPs) of 79 and 140 atoms and a slab. Oxygen atoms (red) are bound to the (111) surfaces (outlined in black for NP140) in hollow sites.

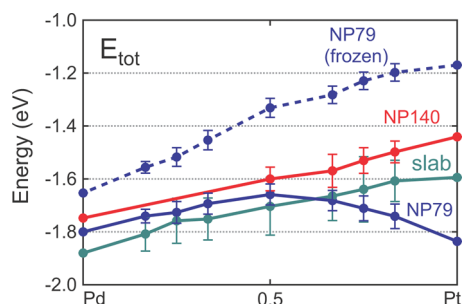


Figure 3. The average oxygen binding energy is shown as a function of Pd/Pt alloy composition. An activity maximum is seen at an intermediate composition for the NP79 structure. This maximum is due to a geometric relaxation of the surface atoms because it is not present in the more rigid NP140 and slab geometries or when the NP79 structure is held frozen upon oxygen binding.

NP79. For NP140, eight oxygen atoms were adsorbed symmetrically on one of the central FCC hollow sites in each facet (shown in Figure 2). Random alloy configurations were generated by randomly shuffling the atom types in a bimetallic NP or slab. A total of 12, 12, and 10 different configurations were used in the NP79, NP140, and slab calculations, respectively.

The average binding energy E_{tot} is defined as the energy change per adsorbed oxygen atom as compared to gas-phase O_2 and the bare metal. Figure 3 shows how this average binding energy changes as a function of Pd/Pt composition. Each data point is averaged over the 12 different configurations (10 for the slab) of the same composition. For the slabs and NP140 geometry, the total binding energy increases monotonically with Pt ratio. The shape of the curve changes dramatically to convex when the particle size is reduced to 79 atoms. While there can be many reasons for which alloys have catalytic properties different

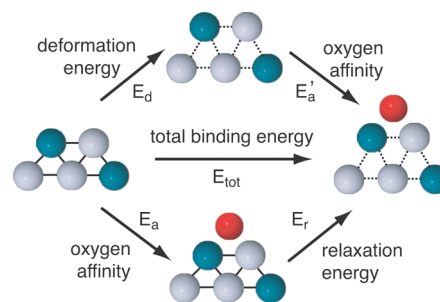


Figure 4. Two ways to decompose the total oxygen binding energy (E_{tot}) by oxygen affinity (E_a or E_a'), metal deformation (E_d), and geometry relaxation energy (E_r).

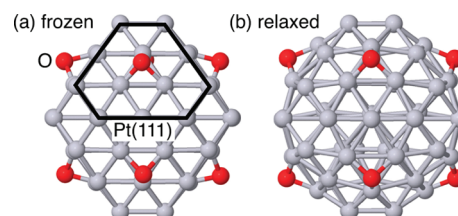


Figure 5. The optimized structure of Pt NP79 bound with eight oxygen atoms where the NP is (a) frozen in the unbound geometry and (b) relaxed to the optimal bound geometry.

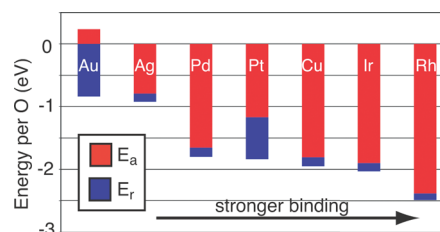


Figure 6. The energies E_r (blue) and E_a (red) for various metal NP79. The sum of E_r and E_a (with sign) in each column is equal to the total oxygen binding energy E_{tot} . Pt and Au show similar binding strengths as the adjacent metals, but the relative contributions to oxygen binding are different.

from their constituent metals, including ligand¹³ and strain effects,¹⁴ this local maximum is related to geometry; it disappears when oxygen is bound to frozen NP79 structures.

As illustrated in Figure 4 and the derivation below, E_{tot} can be decomposed into these two parts

$$\begin{aligned}
 E_{\text{tot}} &= \frac{E_{\text{MO}_x} - E_{\text{M}} - (x/2)E_{\text{O}_2}}{x} \\
 &= \frac{E_{\text{MO}_x} - E_{\text{MO}_x}^{\text{frozen}}}{x} + \frac{E_{\text{MO}_x}^{\text{frozen}} - E_{\text{M}} - (x/2)E_{\text{O}_2}}{x} \quad (1) \\
 &= E_r + E_a
 \end{aligned}$$

where x is the number of bound oxygen atoms, E_{M} is the energy of the bare NP or slab, and E_{MO_x} is the energy of the oxygen-bound NP or slab with the metal atoms either in a relaxed or frozen structure as specified. E_{O_2} is the energy of a gas-phase O_2 molecule. E_r is defined as the energy of geometric relaxation, and E_a is the oxygen affinity to the metal surface. This decomposition

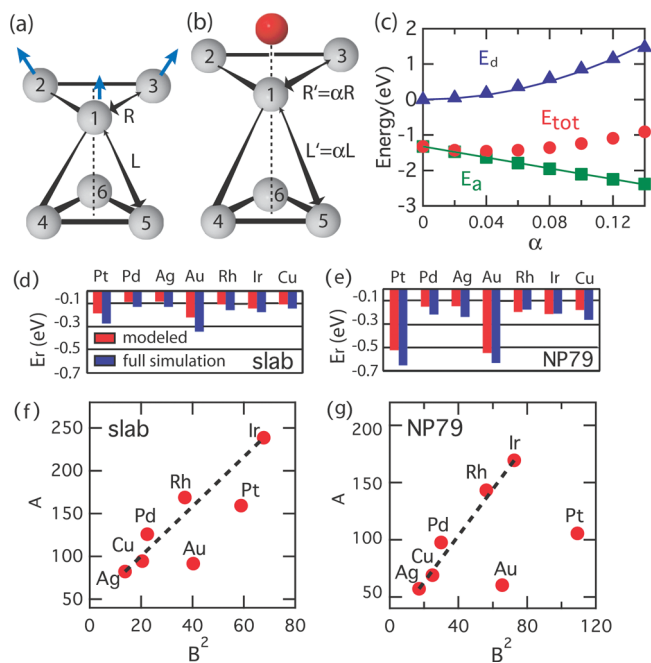


Figure 7. (a,b) A simple geometric model for the deformation induced by oxygen binding. The size of the triangle (R) formed by three FCC hollow atoms (1, 2, and 3) and the interlayer distance L are increased by a factor of α . (c) E_d (blue triangles), E_a (green squares), and E_{tot} (red circles) as a function of α for a Pt slab. Solid curves are the least-squares fit. (d,e) The relaxation energy E_r predicted by the model (red) and from the full simulation (blue) is compared for slab and NP79. (f,g) Scatter plot of corresponding fitting parameters A and B (squared) for various metals. The dashed lines connect Ag and Ir and are used to emphasize how Au and Pt are exceptions to a trend across the metals.

is not unique. E_{tot} can also be expressed as the sum of the metal deformation energy (E_d) and the corresponding oxygen affinity energy to the deformed metal (E'_a). In the following, we focus on the relationships between E_{tot} , E_a , E_d , and E_r in both pure metal and alloy systems.

As shown in Figure 5, eight oxygen atoms bound to the Pt NP79 with frozen and relaxed atoms result in significantly different geometries. According to eq 1, the energy difference between the two structures is equal to (eight times) E_r . The value of E_r is a measure of the metal deformation energy, whereas E_a , the binding energy to the frozen particle, reflects the intrinsic metal–oxygen affinity. The values of E_r and E_a for various metal NP79 are summarized in Figure 6. The result shows that the E_r contribution for most metals is much less than E_a , except for Au and Pt. For metals such as Ag, Pd, Cu, Ir, and Rh, the overall oxygen binding strength is primarily determined by their intrinsic oxygen affinity E_a . The geometric contribution E_r is surprisingly high for Pt and Au, which shows that structure relaxation plays an important role in the oxygen binding process.

To gain more insight into the binding trend, we adopted a simple geometric model to describe the surface deformation caused by oxygen binding. As illustrated in Figure 7a and b, the metal deformation is characterized by an increase in the bond lengths and a lifting of the three FCC hollow atoms to which oxygen binds. The reaction coordinate is quantified simply by the relative increase α of these distances. E_d , E_a , and E_{tot} as a function of α for various metals with slab and NP79 geometry were calculated. The example of a Pt slab is summarized in Figure 7c.

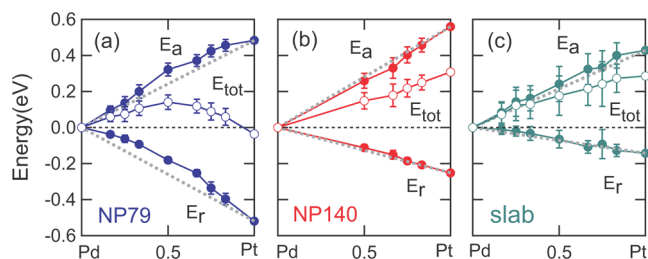


Figure 8. The total oxygen binding energy and the energy decomposition of the Pd/Pt random alloy in the forms of (a) NP79, (b) NP140, and (c) slab at various compositions. For ease of comparison, all of the curves were shifted to 0 at the left. The grey dashed lines represent the linear interpolations from the pure metal data.

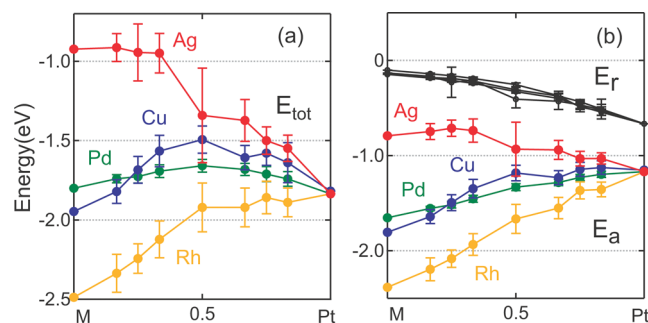


Figure 9. (a) The total oxygen binding energy and (b) the energy decomposition of Pt-based random alloy NP79 at various compositions. The colored E_a curves represent the following types of alloys: Ag/Pt (red), Rh/Pt (yellow), Pd/Pt (green), and Cu/Pt (blue). Because the E_r curves are similar, their colors are kept in black for visual clarity.

To characterize the data, we fit the E_d curves to quadratic forms [$E_d(\alpha) = A\alpha^2/2$] and E_a curves to straight lines [$E_a(\alpha) = B\alpha + C$]. These functional forms are chosen because the deformation energy $E_d(\alpha)$ should follow an elastic model and the oxygen affinity $E_a(\alpha)$ should increase linearly for small deformations, α . As the metal deforms, the increase in E_d is compensated by a stronger oxygen affinity E_a , resulting in a minimum in the total energy $E_{tot}(\alpha)$ for some equilibrium deformation. The magnitude of the deformation will depend on the values of A and B for each metal. We should emphasize that this particular model is not a precise reaction coordinate for any of the metals. However, as summarized in Figure 7d and e, the relaxation energy E_r predicted by this simplified model for slab and NP79 geometry can capture the trend between metals very well. According to this model, the pronounced geometric relaxation in Pt and Au is attributed to a higher gain in E_a (i.e., large B) at a relative lower cost of E_d (small A). In the scatter plots of the two fitting parameters A and B (squared) for various metals (Figure 7f and g), one can readily recognize the unique properties of Pt and Au from the other metals.

The energy decomposition in Figure 8 exhibits strong size dependence in E_r . The change in E_r becomes comparable to that in E_a for the smallest particles, and the effect is significant at high Pt ratio, as inferred from Figure 6. Also, one can see that the E_a and E_r curves of NP79 are not linear but rather have a convex shape. In the Pd-rich region, the change of E_r is relatively small. Therefore, the slope of E_{tot} is determined by the trend of the E_a curve. On the other hand, in the Pt-rich region, the trend of E_{tot} is

dominated by the slope of the E_r curve. The above factors explain why the E_r trend in NP79 reverses at high Pt ratio and looks so different from the curves of NP140 and slab geometry.

Here, we introduce the terms “hard” and “soft” to distinguish whether a metal is prone to deform in response to oxygen binding. In the previous example, we know the geometry relaxation is mainly from Pt, which we consider a soft metal. When a hard metal forms an alloy with Pt, it not only changes the oxygen affinity (E_a) but also makes the alloy harder (E_r). The effect can be observed in other Pt-based alloys. The oxygen binding energy curves and the corresponding energy decompositions for Ag/Pt, Pd/Pt, Cu/Pt, and Rh/Pt NP79 are summarized in Figure 9. According to Figure 6, we know that all four metals are hard but differ in the oxygen affinity. The E_r curves in Figure 9a nicely overlap, which indicates that all hard metals look the same to Pt in terms of how they influence how the alloy deforms, and the trend of the E_r curve can be considered characteristic of Pt. Therefore, the difference in E_a determines the binding trend of these alloys. Among them, Rh has the strongest oxygen affinity, and thus, its binding curve shown in Figure 9a is dominated by E_a . Unlike other metals, the E_a curve of Ag has the same sign of slope as E_r . Both of them are energetically unfavorable when the Ag ratio increases. As a result, the Ag binding curve exhibits the opposite trend to Rh. The E_r curves of Pd and Cu lay in between, and the magnitude of change in E_r is comparable to the change in E_a . Therefore, their binding curves are convex with a peak in the middle at a compromise between the changes in E_a and E_r .

From the above discussion, we know that when the size of a metal particle is small (less than 100 atoms), the geometric relaxation induced by oxygen binding becomes significant for soft metals such as Pt and Au. The overall oxygen binding energy is thus a balance between the intrinsic oxygen affinity and the geometric relaxation energy. Geometric relaxation can significantly stabilize the particle and, for Pt alloys, reduce the ORR activity. One possible way to fine-tune the binding energy is by making an alloy. Our calculations show that by introducing hard metals such as Pd or Cu, their mild oxygen affinity will not change the overall oxygen affinity dramatically, but instead, the binding energy can be adjusted by suppressing the structural relaxation. This mechanism is particularly important for small nanoparticle catalysts.

AUTHOR INFORMATION

Corresponding Author

*E-mail: henkelman@mail.utexas.edu.

ACKNOWLEDGMENT

This work was supported by the Department of Energy under Contract DE-FG02-09ER16090 and the Robert A. Welch Foundation under Grant No. F-160. Computational resources were provided by the National Energy Research Scientific Computing Center and the Texas Advanced Computing Center at the University of Texas at Austin.

REFERENCES

- (1) Besenbacher, F.; Chorkendorff, I.; Clausen, B. S.; Hammer, B.; Molenbroek, A. M.; Nørskov, J. K.; Stensgaard, I. Design of a Surface Alloy Catalyst for Steam Reforming. *Science* **1998**, *279*, 1913–1915.
- (2) Greeley, J.; Mavrikakis, M. Alloy Catalysts Designed from First Principles. *Nat. Mater.* **2004**, *3*, 810–815.

- (3) Ye, H.; Crooks, R. M. Effect of Elemental Composition of PtPd Bimetallic Nanoparticles Containing an Average of 180 Atoms on the Kinetics of the Electrochemical Oxygen Reduction Reaction. *J. Am. Chem. Soc.* **2007**, *129*, 3627–3633.

- (4) Bligaard, T.; Nørskov, J. K.; Dahl, S.; Matthiesen, J.; Christensen, C. H.; Sehested, J. The Brønsted–Evans–Polanyi Relation and the Volcano Curve in Heterogeneous Catalysis. *J. Catal.* **2004**, *224*, 206–217.

- (5) Perdew, J. P.; Chevary, J. A.; Vosko, S. H.; Jackson, K. A.; Pederson, M. R.; Singh, D. J.; Fiolhais, C. Atoms, Molecules, Solids, And Surfaces: Applications of the Generalized Gradient Approximation for Exchange and Correlation. *Phys. Rev. B* **1992**, *46*, 6671–6687.

- (6) Perdew, J. P.; Wang, Y. Accurate and Simple Analytic Representation of the Electron-Gas Correlation Energy. *Phys. Rev. B* **1992**, *45*, 13244–13249.

- (7) Kresse, G.; Furthmüller, J. Efficiency of Ab-Initio Total Energy Calculations for Metals and Semiconductors Using a Plane-Wave Basis Set. *Comput. Mater. Sci.* **1996**, *6*, 15–50.

- (8) Kresse, G. Dissociation and Sticking of H₂ on the Ni(111), (100), and (110) Substrate. *Phys. Rev. B* **2000**, *62*, 8295–8305.

- (9) Kresse, G.; Hafner, J. First-Principles Study of the Adsorption of Atomic H on Ni (111), (100) and (110). *Surf. Sci.* **2000**, *459*, 287–302.

- (10) Blöchl, P. E. Projector Augmented-Wave Method. *Phys. Rev. B* **1994**, *50*, 17953–17979.

- (11) Kresse, G.; Joubert, D. From Ultrasoft Pseudopotentials to the Projector Augmented-Wave Method. *Phys. Rev. B* **1999**, *59*, 1758–1775.

- (12) Monkhorst, H. J.; Pack, J. D. Special Points for Brillouin-Zone Integrations. *Phys. Rev. B* **1976**, *13*, 5188–5192.

- (13) Hammer, B.; Nørskov, J. K. Electronic Factors Determining the Reactivity of Metal Surfaces. *Surf. Sci.* **1995**, *343*, 211–220.

- (14) Kitchin, J.; Nørskov, J. K.; Barteau, M. A.; Chen, J. G. Role of Strain and Ligand Effects in the Modification of the Electronic and Chemical Properties of Bimetallic Surfaces. *Phys. Rev. Lett.* **2004**, *93*, 10240–10246.